Numerical Modelling of Microstructure Inhomogeneity to Reproduce Experimentally Observed Scatter in Fretting Fatigue Lifetimes

Grzegorz Glodek[a,*], Ander Nazabal[b], Iñigo Llavori[b], Reza Talemi[a]

[a]Department of Materials Engineering, KU Leuven, 3001, Leuven, Belgium
[b]Mechanical and Industrial Manufacturing Department, Mondragon Unibertsitatea, Loramendi 4, 20500 Mondrag´on, Spain
*Correspondence: grzegorz.glodek@kuleuven.be

Abstract: Experimental fretting fatigue lives exhibit large degree of scatter. One of the aspects behind this is the microstructural inhomogeneity which affects the stresses in the material. Variance in stress values can greatly impact crack initiation speed, leading to changes in fretting fatigue lifetimes, as well as the crack propagation behaviour. This research aims to study this issue in more detail and recreate the experimentally observed scatter using numerical modelling. In this work, Voronoi tessellation is used to simulate microstructural topologies of low carbon steel, where each grain is assigned elasto-plastic properties at random, from a predetermined range. In total, 60 finite element models are created and the effect of microstructural inhomogeneity on fretting fatigue lifetime dispersion is evaluated using a Continuum Damage Mechanics approach. Additionally, crack propagation is studied with XFEM combined with Smith-Watson-Topper fatigue parameter to determine crack path under multiaxial, non-proportional loading conditions. For both crack initiation and propagation investigation, the Theory of Critical Distances is applied to overcome the effect of high stress gradients. Simulation results show that microstructural inhomogeneity has significant impact on the contact stress distributions and subsurface stress and strain fields. Scatter observed in the predicted lifetimes matches well with that observed in practical experiments and is used to propose a design curve for the studied material. The applied crack path prediction approach captures the variance in crack paths originating from microstructural inhomogeneity and shows good correlation with reference experimental results at low bulk stress levels.

Keywords: Fretting Fatigue; Numerical Modelling; Voronoi Tessellation; Continuum Damage Mechanics; XFEM;

Nomenclature

Abbreviation

CDM – Continuum Damage Mechanics
COF – Coefficient of Friction
FE – Finite Element
FEM – Finite Element Modelling
IH-FFM – Inhomogeneous Fretting Fatigue Model
MEMS – Microelectromechanical System

PEEQ – Equivalent Plastic Strain
RVE – Representative Volume Element
SWT – Smith-Watson-Topper
TCD – Theory of Critical Distances

Symbols

B – Threshold Parameter for Lifetime
b – Isotropic Hardening Exponent
C – Threshold Parameter for Stress Level
D – Damage Parameter
D_c – Critical Damage Parameter
$\breve{E}$ – Effective Young's Modulus
F – Force
k – Fatigue Strength Exponent
K_{th} – Crack Propagation Threshold
L – Critical Distance
m – Material Constant
N – Number of Fatigue Cycles
N_f – Number of Fatigue Cycles at Failure
V – Normalized Weibull Distribution Variable
δS – Intersection Area Between the Plane and the RVE
δS_d – Area of Defects Situated in the δS
ε – Strain
ϵ_n – Normal Strain
θ – Crack Propagation Angle
σ - Stress
$\tilde{\sigma}$ – Effective Stress
σ_a – Stress Amplitude
σ_f' – Fatigue Strength Coefficient
σ_m – Mean of the Cyclic Stress
σ_n – Normal Stress
σ_o – Fatigue Limit
σ_r – Resistance Stress
σ_u – Ultimate Tensile Stress
σ_v – Von Mises Stress
σ_0 – Material Constant

1. Introduction

Fretting is defined as relative, oscillatory, tangential movement of minute displacement amplitude between two bodies in contact. This often results in high cyclic stresses and leads to formation of surface damage. If fluctuating bulk loading is present, fretting fatigue occurs, which, due to the generated surface damage, greatly speeds up the crack initiation process and reduces the lifetime of affected components. Fretting fatigue is the cause of early failure in numerous applications such as bolted joints [1,2], overhead conductors [3], bearing shafts [4], dovetail geometry connections common in turbine assemblies [5], or even tiny microelectromechanical systems (MEMS) [6]. The widespread nature of this issue not only generates economical losses but also poses a significant threat to human health and safety [7]. Because of that, in the past years, significant effort has been made to study how different parameters affect components subjected to fretting fatigue in order to better understand the failure mechanism and develop potential solutions for mitigating this issue [8–10].

One of the most important parameters affecting the fretting fatigue response is the material and its microstructure, which has led many researchers to investigate this topic in great detail. Microstructure of the material is instrumental in determining its applicability in different scenarios as two metal alloys with the same composition can have different mechanical properties, depending on the microstructural topologies [11]. The effect of grain size, shape and distribution is especially important when it comes to fretting fatigue due to highly localized nature of the stress concentrations at contact edges, and the impact of the crack initiation process on the total lifetime. Further study into this field could help explain high scatter in fretting fatigue lives often observed in experimental investigations. Nesládek et al. [12] have performed a series of fretting fatigue tests on chromium steel in order to investigate the accuracy of different lifetime prediction methods. Fretting fatigue lives they have reported exhibit significance variance in total lives, which is especially pronounced at lower bulk stress levels where the lifetimes differ by more than an order of magnitude. Wang et al. [13] in their work studied the fretting fatigue response of AlSi9Cu2Mg aluminium alloy. In this case the scatter in fretting fatigue lives at the same levels of alternating stress is also clearly visible, but there are no noticeable differences between the respective levels and the scatter remains uniform for all stress values.

One of the early experimental investigations into the effect of microstructure on fretting fatigue is the research by Venkatesh et al. [14] who studied, among other things, the effect of microstructure of Ti-6Al-4V titanium alloy on the fretting fatigue lifetime. Obtained results showed that a martensitic microstructure resulted in longer fretting fatigue lifetimes compared to other investigated microstructures, between which no significant differences were observed. Venkatesh et al. noted that the martensitic microstructure exhibited higher hardness, which in addition to higher resistance to crack propagation [15], likely contributed to its better performance in the experiments. Mall et al. [16] demonstrated in a separate investigation that a duplex microstructure of Ti-6Al-4V exhibited greater resistance to fretting fatigue than a lamellar microstructure. The worse performance was attributed to the lower resistance to crack initiation observed in the lamellar microstructures. Later work by Hong et al. [17] investigated the Inconel 690 nickel superalloy and showed that hardness has little effect on the degree of wear, but highlighted a strong influence of the grain size. Smaller grain size samples exhibited significantly higher mass loss which was attributed to the presence of chromium carbides in grain boundaries promoting crack formation and propagation. As grain size increased, fewer crack initiation sites on smaller grain boundaries resulted in increased wear resistance. Mall et al. [18] investigated a different type of nickel superalloy, specifically IN100, and focused on the effect of microstructure on fretting fatigue life. Their findings showed that the fine microstructure offers longer fretting fatigue lives as opposed to coarse microstructure due to higher crack initiation resistance, which is in line with the fact that crack nucleation plays a major role in fretting fatigue process.

In parallel to the experimental investigation into the effect of microstructure on fretting fatigue response significant effort has been made to simulate different microstructures using Finite Element (FE) software. Some of the earliest works by Goh et al. [19–21] employed the crystal plasticity theory to simulate the grains of Ti-6Al-4V and investigate the influence of contact load, stress amplitude, microstructural texture and COF on the fretting fatigue response of the material. This comprehensive research produced results that match the experimental results well and highlight the importance of phenomena such as ratchetting of plastic strains for better understanding of the fretting fatigue process. Dick et al. [22,23] extended this approach and created 3D crystal plasticity models of Ti-6Al-4V in order to more accurately simulate the behaviour of the material. The obtain results reaffirm the importance of strain ratcheting in the fretting fatigue process and provide valuable insights into the crack nucleation process, showing that multiple crack can coalesce and cause material separation but isolated cracks near contact edges have the capacity to grow deeper into the material. More recently McCarthy et al. [24] have combined a crystal plasticity model of Ti-6Al-4V with a microstructure-sensitive fatigue indication parameter to better understand the crack initiation process. The developed approach could accurately simulate the crack nucleation behaviour under partial slip and have been adapted to enable a new methodology for wear prediction.

Apart from the effect different microstructures have on the physical response of the material, it is just as important to study microstructural inhomogeneity, where different grains of the same material exhibit different properties based on their spatial arrangement and composition. This phenomenon is especially applicable to steels, which caused many researchers to study the relation between microstructural inhomogeneity and physical properties in great detail [25–27]. Already Goh et al. [19] in their earliest work studied the effect different microstructural textures of Ti-6Al-4V have on the fretting fatigue response and found a high variance in the maximum cumulative effective plastic strain, depending on the simulated texture. The research by Mayeur et al. [28], who simulated the 3D crystallographic texture of Ti-6Al-4V, provides further information into this topic. The basal texture shows uniform subsurface plastic strain distributions, with peak values always located at the surface and close to contact edges. On the other hand, the transverse and basal/transverse textures have heterogenous plastic strain distributions and the location of the peak value depends on the tangential load. Zhang et al. [29] investigated the same three textures, in addition to grain size and distribution, using a full 3D models of fretting fatigue contact. The obtained results reveal negligible effect of the grain distribution on fretting fatigue life, but show that the smaller grain size and transverse and basal/transverse textures provide greater resistance to fretting fatigue. McCarthy et al. [30] have focused on a different material and researched the effect of microstructural inhomogeneity in 316L steel using a crystal plasticity model. Presented results have clearly shown the scatter in lifetimes obtained based on models with different, randomly assigned grain orientations. They have highlighted the importance of considering the relative magnitudes of contact width, slip amplitude and grain size when estimating the fretting fatigue crack nucleation life. Ashton et al. [31] have studied the effect of grain size on fretting fatigue response of cobalt chromium alloy using a 3D FEM that incorporated crystal plasticity. The results have shown that with a decrease in the grain size, the average predicted life and the scatter in predictions decrease. This is attributed to the increased likelihood of unfavourable grain combinations near the contact interface, which create conditions that promote crack initiation. In a subsequent study [32], the authors used improved FE model to simulate the microstructure of ferritic-pearlitic steel to predict the location and initial direction of crack propagation in fretting fatigue. The model also accurately captures the length-scale effects, and shows that small contact widths are more favourable in fretting fatigue due to a higher degree of slip system hardening caused by a large density of geometrically necessary dislocations.

In addition, it is important to pay special attention to the relationship between the material microstructure and the crack initiation process. McDowell and Dunne [33] have done significant work in this area and showed that the microstructure of the material can have a significant impact on the fatigue crack initiation. They proposed different fatigue indication parameters to study this issue, such as accumulated plastic strains or the Fatemi-Socie parameter based on plastic shear strains. Sangid [34] highlighted the importance of the dislocation motion combined with slip of the crystalline lattices as the main mechanism behind crack initation in face centre cubic metals. As the dislocation occur preferentially on low energy pathways, the accumulation of slip leads to formation of persistent slip bands which are responsible for a build-up of defects at the grain boundaries and promote crack initation along those slip bands. In his review, Sangid evaluated different methods of simulating the effect of persistent slip bands and methods of correlating them with the crack initation process. Sweeney et al. [35] showed that cyclic effective plastic strain and peak accumulated slip are capable of predicting crack nucleation locations accurately, but the simulated cracks did not initiate along the dominant slip directions but followed the grain boundaries. Additionally, the effect of length scale effects was shown to have a significant impact on the investigated fatigue indication parameters over the course of many cycles (high-cycle fatigue).

Other researchers have focused on capturing the scatter in fretting fatigue lives originating from microstructure randomness. Both Slack et al. [36] and Walvekar et al. [37] have investigated the effect of microstructural inhomogeneity on fretting fatigue response. Slack et al. [36] have used FEM with Voronoi tessellation to simulate the microstructural inhomogeneity and predict fretting fatigue life using a critical plane-based approach. Their results have successfully captured variability in predictions, and Weibull statistical model have been used to show that with the highest levels of scatter have occurred at low load levels. Walvekar et al. [37] have proposed a new approach, which combined Voronoi tessellation and Continuum Damage Mechanics (CDM) to predict fretting fatigue lifetime. Their FEM simulations have incorporated the effect of material inhomogeneity on lifetime predictions and have been validated with practical tests, indicating good agreement between experimental data and numerical predictions. However, since each test was conducted at a different load level, it was not possible to evaluate the degree to which the scatter in lifetime estimations matches the actual scatter in lifetime caused by nonuniform material grain properties.

The objectives of this work focus on the effect of microstructural inhomogeneity in medium carbon steel on the fretting fatigue response. Specifically, the effect of random grain shapes and sizes, and random properties of the grains including the elastic modulus and elasto-plastic behaviour are investigated with the aim of recreating the scatter in experimental data, characteristic for retting fatigue tests. This is achieved with FEM approach where Voronoi tessellation is used to model the grains of S45C steel with varying dimensions, and for each of those grains' material properties are selected at random, from a predetermined range. The results of the simulations are compared to a model with homogenous material properties in order to better understand the effect of randomness in the material microstructure on the distribution of contact and subsurface stresses. The results of the FE simulations are utilized in the lifetime estimation methodology based on the CDM and the Theory of Critical Distances (TCD). Accuracy of the obtained predictions is compared against reference experimental data and the scatter in lives is quantified using Weibull statistics. The simulations are taken one step further and the XFEM capability of the ABAQUS software is used to predict the crack propagation paths using a novel approach based on the critical plane principle and multiaxial damage parameter. The effect of microstructure randomness on crack propagation paths is evaluated and a comparison is made with reference experimental result.

2. Lifetime Estimation Methodology

The effect of microstructure randomness on the fretting fatigue lifetime of S45C steel is investigated by performing lifetime estimation using the CDM methodology. This approach is based on the law of thermodynamics and uses bulk material properties to simulate damage accumulation in the studied assembly. Past research shows that the CDM methodology can be successfully applied to fretting fatigue problems. Glodek et al. [5] have used it to predict the lifetime of dovetail geometry components based on experimental coupon scale data, while Talemi [8] has utilized the CDM approach to study the effect of non-proportionality of stresses at contact and subsurface pores in additively manufactured AlSi10Mg alloy [9], on fretting fatigue lifetime.

The theory of CDM was first introduced by Kachanov [38] and it defines a specific damage parameter *D* which represents the accumulation of damage in the form of micro-voids in the material. Those cavities reduce the structural integrity of the material and reduce its ability to bear loads. As the damage parameter D depends on the orientation it is defined as a tensor but by using the application of the Representative Volume Element (RVE), Kachanov [38] showed that it can be defined as a scalar parameter obtained with following equation:

$$D = \frac{\delta S_d}{\delta S} \tag{1}$$

δS is the area of the intersection between the plane and the RVE and δS_d is the total area of all the microscopic defects which are situated in the δS. For an ideal material with no internal voids, $\delta S_d = 0$, but as damage is accumulated, e.g. due to fatigue loading, δS_d will begin to increase, together with the parameter D, tracking the accumulation of damage in the material. Failure occurs when D reaches a critical value for the given material, often taken as 1, which corresponds to complete fracture. Using the damage parameter D it is possible to define an effective stress $\tilde{\sigma}$:

$$\tilde{\sigma} = \frac{F}{\delta S - \delta S_d} = \frac{F}{\delta S(1 - \frac{\delta S_d}{\delta S})} = \frac{\sigma}{1 - D}, \tag{2}$$

which can be related to the effective strain, and by application of the Hook's law, it can be used to track the evolution of the effective Young's modulus of the material as damage accumulates:

$$\tilde{\sigma} = \breve{E}\varepsilon, \tag{3}$$

$$\tilde{\sigma} = (1 - D)E\varepsilon, \tag{4}$$

$$\breve{E} = (1 - D)E \tag{5}$$

Lemaitre and Chaboche [39–41] used the CDM theory introduced by Kachanov [38] to develop a number of constitutive equations for the damage accumulation, able to estimate the lifetime of components under low and high cycle fatigue, fatigue creep and ductile fracture. This study uses the equation for high cycle fatigue, proposed by Bhattacharya and Ellingwood [42] as past research shows it provides accurate estimations in the case of fretting fatigue loading [8,9]. The equation takes the following form:

$$\frac{dD}{dN} = \left[\frac{\sigma_a}{\sigma_r(1 - D)}\right]^m, \tag{6}$$

where *N* is the number of cycles, σ_a is the stress amplitude of the damaging stress, *m* is a material constant and σ_r is the resistance stress which is defined as follows:

$$\sigma_r = \sigma_0\left(1 - b\frac{\sigma_m}{\sigma_u}\right) \tag{7}$$

Here σ_0 and *b* are material constants, σ_m is the mean of the applied cyclic stress and σ_u is the ultimate tensile stress. By integrating Equation (6) from 0 to number of cycles to failure N_f and from *D* = 0 to the critical value of *D*, which is taken as 1 in this research and corresponds to fully fractured material, it is possible to correlate the magnitude of σ_a with N_f. Performing this integration gives:

$$\int_0^{N_f} dN = \int_0^{D_c} \left\{\frac{\sigma_r(1 - D)}{\sigma_a}\right\}^m dD, \tag{8}$$

$$N_f = \left[\frac{\sigma_r}{\sigma_a}\right]^m \left(\frac{(1 - D)^{m+1}}{-(m + 1)}\right)_0^1, \tag{9}$$

$$N_f = \frac{1}{(1 + m)}\left[\frac{\sigma_r}{\sigma_a}\right]^m, \tag{10}$$

where σ_r is defined as in Equation (7) and *m* is a material constant, both of which can be calibrated using the plain fatigue of the material data taken from literature.

The value of σ_a can be obtained based on the results of FE simulation, but selection of the value which will provide the most representative results proves to be challenging in the case of fretting fatigue. The research shows that fretting fatigue cracks initiate predominantly at the edges of contact due to high stress concentrations and the damaging effect of low magnitude slip [43–45]. But the presence of high stress gradients in this region [46], combined with the rapid changes of the stress fields during a fretting fatigue cycle [47] can lead to over-conservative lifetime predictions. In other to solve this problem many researches incorporate TCD in their fretting fatigue lifetime estimations [48,49]. TCD, which was developed by Taylor [50], defines a material length scale L, referred to as critical distance, which is used to predict fracture and fatigue behaviour. TCD is often applied to problems containing short-cracks, small defects, or sharp notches, where it is used to define a condition for failure of the material, based on the stress fields around the stress concentration inducing defect. For fatigue problem, the value of L can be obtained using the following equation:

$$L = \frac{1}{\pi}\left(\frac{\Delta K_{th}}{\Delta \sigma_o}\right)^2, \tag{11}$$

where ΔK_{th} is the crack propagation threshold and $\Delta \sigma_o$ is the fatigue limit of the material.

3. Finite element modelling

3.1 Voronoi partition finite element model

Evaluation of the fretting fatigue conditions is done by creating a FE model in a simulation software ABAQUS. Developed 2D model, showed in Figure 1, is based on the work by Noraphaiphipaksa et al. [51] and represents the geometry of the fretting fatigue set-up with bridge-type, cylindrical contact pads. Due to the vertical and horizontal symmetry of the test set-up it is possible to model only one quarter of it and fix the displacements of the components with X- and Y-symmetry boundary conditions. The model consists of three parts: the fretting pad, the bulk fatigue specimen and the Voronoi partition region, which is a separate part in contact with the fretting pad and attached to the bulk fatigue specimen using tie constraints. In order to simulate the microstructural grains of S45C steel, the principle of Voronoi tessellation is used. Voronoi tessellation, or a Voronoi diagram is a partition of a plane into regions, each consisting of points closest a finite number of defined points often referred to as seeds. The distribution of the seeds on the plane defines the size and shape of those regions, which are called Voronoi cells. This property makes it possible to simulate material grains which have random shapes and sizes. The seeds of the Voronoi tessellation can be understood as the nucleation points in the crystallization process of a metal, under the assumption that all grains grow at the same rate.

A dedicated Python script has been developed to generate Voronoi tessellation in ABAQUS software. The size of the Voronoi cells is based on the average grain size of the S45C steel, which is taken as 20 µm [52], which resulted in 150 cells in the Voronoi partition region. In total, 30 of such mesh regions were generated, each with a different Voronoi diagram representing different distributions of the material grain structure.

Figure 1. *The loading and boundary conditions, as well as the mesh structure of the Voronoi tessellation FE model representing the fretting fatigue testing set-up. The exact dimensions of all parts can be found in* [51].

Two different meshing strategies are applied in the model. The meshes in the fretting pad and the fatigue specimen are generated using Coreform Cubit software which allows for a smooth transition from a coarse mesh to very fine mesh at and near the contact area, which is necessary to obtain accurate stress distributions. This approach reduces the total number of elements and speeds up the FE simulation which is crucial in this study since a large number of simulations has to be conducted in order to capture the scatter in the results. In the pad, the mesh decreases from 250 µm down to 5 µm at the contact interface, a value which was obtained based on the convergence study and matches the one used by Noraphaiphipaksa et al. [51]. In the specimen the mesh size is larger and varies from 300 µm close to the edges of the part to 5.5 µm next to the space where the Vornoi partition region is positioned. The mesh in the Voronoi partition region is generated within ABAQUS software directly, with an element size equal to 4 µm. For all parts, quadrilateral, 4-node, plane strain elements with reduced integration (CPE4R) are used.

Contact between the fretting pad and the fatigue specimen is defined as the surface-to-surface contact pair where the master surface is assigned to the pad and the slave surface is assigned to the Voronoi partition region. The contact property is defined using the penalty method for the tangential behavior, with coefficient of friction equal to 0.6, and default, hard contact for the normal behavior. In total, six loading steps are simulated, starting with application of pressure to the contact pads equal to 17.136 MPa, equivalent ti the 856.8 N clamping force used in the experiments [51], which is held constant throughout the entire simulation. In the next step, maximum fatigue load is applied to the right side of the specimen and the next four steps are meant to simulate a fatigue cycle with the stress ratio value R_s equal to -1. The load is lowered to 0 from the maximum, then the loading direction is reversed and the sample is put under compression. Following that the load is increased back to 0 and in the last step the maximum load value is applied as tension again. In total 13 load levels are considered, covering the same total range as in [51], starting from 180 MPa and increasing by 10 MPa up to 300 MPa.

The fretting pad and the fatigue specimen are assigned only elastic material properties as initial simulations revealed that no plastic deformations occur in those elements during the fretting fatigue loading cycle. The Young's modulus of S45C steel is taken as 210 GPa and the Poisson's ratio is equal to 0.3, as reported in [51]. As for the Voronoi partition region, where elasto-plastic properties are used, the material data is taken from literature [53] where the same grade of steel is used. The extracted stress-strain data is used to obtain true stress-plastic strain relationship and serves as an input for isotropic hardening material definition in ABAQUS. In order to introduce variance in the material properties of different grains, the Young's modulus is varied from 180 GPa to 280 GPa in steps of 10 GPa. This creates a variation in the local elastic modulus which is shown in Figure 2 (a) for the grains at the contact surface. The selected range of the Young's modulus is based on the the research performed by Qiu et al. [54], where a similar range have been reported for different grains of steel, as shown in

Figure 2 (b). In this work an extreme case is being considered and, in order to reflect this in the simulations, the Young's modulus range is shifted accordingly.

Figure 2. *(a) The distribution of the local elastic modulus on the contact surface of the Voronoi partition region in the FE fretting fatigue model and (b) experimentally determined distribution of the local elastic modulus on the surface of a steel specimen* [54].

Moreover, values of the true stress for each true strain are changed proportionally along with the changes in the Young's modulus, so for an increase from 210 GPa to 220 GPa, which corresponds to an increase by a factor of 1.048, the values in the extracted stress strain curve are increased by the same factor as well. This process is repeated for each of the 11 considered values of the Young's modulus, which leads to a creation of 11 stress strain curves, which are shown in Figure 3. The exact values of the Young's modulus and the corresponding yield and ultimate tensile stresses are listed in Table 1. Using the created materials, each simulation run is prepared automatically utilizing the Python scripting capabilities of ABAQUS. A code is developed which assigns one of the 11 material properties at random to each grain. In the next step, the script applies one of the randomly selected load level values to the fatigue specimen, which completes the model, and generates an input file which is subsequently used to perform the simulations. Using this procedure 60 input files are generated, two for each of the previously prepared Voronoi partition regions. Since the Young's modulus and the elasto-plastic behaviour are assigned randomly to each grain, and the load level is chosen at random, each input file is different and generates unique set of results.

Figure 3. *Stress strain curves used to simulate the variation of mechanical properties of different grains in S45C steel.*

Table 1. *Properties of the different material parameters assigned to the microstructural grains.*

3.2 Application of the CDM lifetime prediction approach

In this research, CDM is combined with TCD, which is used to define a critical grain under the contact surface, as shown in Figure 4. First, the most likely crack initiation spot is found at the edge of contact using the maximum value of the in-plane principal stress. Maximum value is used instead of the maximum range because the principal stress range considers compressive stresses, which are believed to not contribute to the crack initiation process in the same capacity as tensile stresses. Using maximum value of principal stresses avoids the uncertainty related to this issue, and provides results consistent with the results reported in [51]. Moreover, similar approach has been successful in the past study on fretting fatigue [55]. Next, a line with length equal to half of the critical distance $L/2$ is drawn, starting in the determined crack initiation location and at an angle equal to the crack initiation angle, which is obtained based on the experimental data taken from [51]. In the following step, the grain with its centre closest to the end of that line is found and selected as the critical grain. The in-plane principal stresses are averaged over the entire grain area at two points in time during the fretting fatigue loading cycles – when the stresses are at the maximum and the minimum levels. With those two values, the amplitude of the in-plane principal stress in the critical grain is calculated and used as the value of σ_a in Equation (10).

Using the average values of in-plane principal stresses within a grain can circumvent the issue of stress singularities that arise at grain edges, which result from the discrepancy in material properties at geometric discontinuities such as the edges of the simulated Voronoi partition cells. The issue of stress singularities has been first researched by Williams [56,57] in cases such as sharp corners or cracks at bi-material interfaces. In case of FEM, as the mesh becomes more refined, the stress values at singularities tend towards infinity which can cause simulation convergence issues and lead to unrealistic results. In this research no numerical or compatibility errors were encountered during the FE simulations. As for the precision of the lifetime estimations, it was observed that for a decrease in mesh size from 8 µm to 4 µm, the average principal stress in each grain changed by less than 1%. Therefore, further grain refinement is unlikely to have a significant impact on the accuracy of the predicted fretting fatigue lifetimes and the effect of stress singularities is negligible.

Figure 4. *Determination of the critical grain for the extraction of the damaging stress used in the lifetime estimation process.*

3.3 XFEM crack propagation

In addition to the study on the effect of microstructural inhomogeneity on the fretting fatigue lifetime estimation, the effect on crack propagation is investigated as well using the XFEM technique available in ABAQUS. Traditional methods of FE based fracture modelling make it possible to simulate crack growth only along predetermined boundaries. XFEM removes this limitation and gives the possibility to model bulk fracture, and allows for the crack to be located in the element interior. The other benefit of the XFEM technique is its independence from the generated mesh, therefore there is no need to re-mesh the FE model for each stage of crack propagation. In order to facilitate the use of this technique for a large number of models, a Python script for ABAQUS was created, which makes it possible to easily select the crack initiation location and direction, the initial crack length, the number of propagation steps, and the methodology used for determining the crack propagation direction.

The crack propagation simulations are conducted for a selection of 12 fretting fatigue models, each with different Voronoi partition region and randomly assigned grain properties, and four different bulk stress levels covering the entire studied range: 180, 210, 250 and 300 MPa. In addition, the effect of crack face contact property definition on crack propagation is investigated. The simulations are performed once with frictionless tangential behaviour and another time with COF = 0.1. As bulk fatigue loading acts perpendicularly to the expected crack propagation path, little tangential movement of the crack faces is expected and frictionless contact simulations can be used to validate the proposed approach. Simulations with COF = 0.1 are performed to evaluate if the introduction of tangential friction affects the crack propagation paths obtained using proposed approach. The normal contact behaviour is kept as hard contact. For each of the conducted simulations the crack initiation point is the same as in the lifetime estimation study and is based on the maximum value of the in-plane principal stress during one fatigue cycle, while the initial crack angle is kept constant at 111°

[51]. The initial crack length and the crack propagation increment, which is the distance the crack is extended for in each simulation step, have been selected based on an initial study aimed at optimizing the accuracy and the computational time required for the crack propagation simulation. Based on this study, both the initial crack length and the crack propagation increment were selected to be 20 µm. As a consequence of this, the total number of propagation steps was selected to be 10 in order to cover the entire depth of Voronoi partition region, which is equal to 200 µm.

The method used to predict the crack propagation path uses the Smith-Watson-Topper (SWT) multiaxial damage parameter. The value of the SWT parameter can be calculated using the following equation:

$$SWT = \frac{\Delta\epsilon_n}{2}\sigma_n \tag{12}$$

$\Delta\epsilon_n$ is the normal strain amplitude on a material plane where this value is maximum. In this research this plane is defined as the critical plane and σ_n is the maximum normal stress acting on that plane. The SWT based procedure for crack propagation prediction used in this research is based on the work by Navarro et al. [58], which was later refined by Erena et al. [4] and Pinto et al. [10], and is depicted in Figure 5.

The first step is conducting the simulation with the initial crack, with the dimensions of the crack defined based on the experimental result from the work in [51]. Next, following the approach proposed by Pinto et al. [10], a point at a distance of $L/2$ from the crack tip and along the crack direction is found, where L is the critical distance as defined by Equation (11). The stresses and strains for the determination of the crack propagation direction will be evaluated at this point. This reduces the effect of high stress gradients near the crack tip on the predictions and results in a smoother crack path. The crack propagation direction is assumed to coincide with the critical plane as defined for the SWT parameter, and so the material plane where the $\Delta\epsilon_n$ is the highest. Therefore, the magnitude of $\Delta\epsilon_n$ is calculated in the critical point for each possible angle between 0° and 180°, with steps of 1°.The angle at which the value of $\Delta\epsilon_n$ is maximum is taken as the crack propagation angle θ, and the FE model is updated by modifying the geometry of the crack, using the value of θ and a predefined crack propagation distance. This process repeats until the selected number of propagation steps have been simulated.

Figure 5 *Schematic representation of the methodology used for crack propagation path prediction.*

4. Results and Discussion

4.1 The effect of grain inhomogeneity

The first FE simulations were conducted using homogenous elastic and elasto-plastic material properties in order to validate the developed model and create a reference data set. Figure 6 (a) shows the contact pressure distribution at a bulk stress value of 300 MPa for purely elastic and elasto-plastic model. The pressure distribution in the elastic model matches the analytical solution obtained using equation for Hertzian contact, the semi contact width a is equal to

0.14 mm and the maximum value is equal to 571.6 MPa. The contact pressure distribution for the elasto-plastic simulation reveals that the half contact width a is higher than in the case of elastic model, equal to 0.18 mm, and the contact pressure distribution is more complex. The maximum value is equal to 455.58 MPa and the contact pressure values are higher at the trailing edge and smaller at the leading edge, which is likely caused by the deflection of the bridge geometry pads. In Figure 6 (b) the contact pressure distributions of the homogenous and inhomogeneous elasto-plastic models are compared with each other. The introduction of the grain inhomogeneity not only has a significant impact on the stress distribution, with irregular peaks and valleys in the stress values depending on the E modulus of the grain in contact, but also affects the contact width, increasing the value of a to 0.20 mm. This corresponds to a 43% increase compared to the elastic model and 11% increase compared to the homogenous elasto-plastic model.

Figure 6. *Contact pressure distribution in the specimen for elastic and homogenous elasto-plastic models compared with the analytical solution (a) and contact pressure distribution in the homogenous and inhomogeneous models (b).*

Figure 7 (a) shows the distribution of the shear stress at the contact edge for the homogenous model at different values of the maximum bulk stress. At maximum bulk stress of 180 MPa, the stick condition in the middle of contact is clearly visible, with slip zones close to the contact edges, a typical stick-slip condition for fretting fatigue. Increasing the bulk stress leads to a decrease in the stick area and above the bulk stress value of 240 MPa the stick area is no longer visible, which signifies that full sliding occurs at the maximum stress level during the fretting fatigue loading cycle. With the increasing values of bulk stress, the half contact width increases as well, from 0.15 to 0.18 mm but the maximum absolute stress value decreases, from 285.87 to 273.35 MPa. The graph in Figure 7 (b) shows the shear stress distributions for the simulations with material grain inhomogeneity. It is important to point out that 2 out of the 60 conducted simulations failed to converge and so the results are reported for the successfully completed 58 simulation. One can see the significant effect the randomness in grain distribution and mechanical properties have on the obtained results. The average contact half width is equal to 0.19 ± 0.01 mm, with the maximum equal to just above 0.21 mm and minimum equal to 0.16 mm. The range of the absolute maximum shear stress values is high as well, from 240MPa to 352 MPa, and when to the homogenous simulations the increase in the highest maximum value is quite significant at 23%.

Figure 7. *Distribution of shear stress at the contact edge of the specimen, at the maximum bulk stress level, for a homogenous (a) and inhomogeneous (b) fretting fatigue models.*

It was found that, when it comes to the slip amplitude the effect of the microstructure randomness is less pronounced. Figure 8 (a) shows the slip amplitude at contact for the homogenous model at maximum stress levels during the loading cycle. With increasing levels of bulk stress, the slip at the edges of contact increases as well and reaches 2.8 µm at the leading edge in the positive x direction (shown in Figure 1) and 3.8 µm in the negative x direction. In case of the inhomogeneous model, for which the results are shown in Figure 8 (b), the maximum slip at the leading edge is equal to 2.9 µm, while at the trailing edge it is 3.7 µm.

Figure 8. *Distribution of slip amplitude at the contact interface between the specimen and the pad, at the maximum bulk stress level, for a homogenous (a) and inhomogeneous (b) fretting fatigue models.*

The effect of the grain inhomogeneity was observed to be the highest in case of the tangential stress distribution at the contact interface. In case of the homogenous model, there is very little difference in the tangential stress values for different bulk stress levels as shown in Figure 9 (a), the average of the stress values at the leading edge is equal to 506.5 ± 5.4 MPa. The only noticeable difference is the location of the maximum stress value, related to the width of contact area, and the difference in values in the middle of contact for lower bulk stress levels, caused by sticking. On the other hand, in case of the inhomogeneous model for which the results are presented in Figure 9 (b), the maximum value of the tangential stress at the leading contact edge varies from 423 MPa up to 587 MPa depending on the grain inhomogeneity which amounts to 15.4% decrease or 17.2% increase in relation to the homogenous model. This difference is especially significant since the tangential stress at the contact edge is one of the main factors driving the crack initiation and early crack propagation. Therefore, depending on the grain inhomogeneity the fretting fatigue lifetime of the affected components can vary greatly.

Figure 9. *Distribution of tangential stress at the contact interface between the specimen and the pad, at the maximum bulk stress level, for a homogenous (a) and inhomogeneous (b) fretting fatigue models.*

Finally, the effect of the grain inhomogeneity is investigated in terms of the equivalent plastic strain under the contact surface. Contour plots shown in Figure 10 show the equivalent plastic strain distribution for a homogenous elasto-plastic model and a selection of inhomogeneous elasto-plastic models with different maximum bulk stress values. One can immediately see that in the homogenous model the plastic strains are more evenly distributed, with higher values near the, surface closer to the leading edge and a larger yielded area further beneath the surface at the trailing edge. In case of the inhomogeneous models, the equivalent plastic strain is closely related to the properties of the individual grains, with weaker grains yielding before the stronger ones. This results in a creation of paths with significant plastic strain, which could create channels along which cracks would preferentially propagate, as marked with the arrows in Figure 10 for the bulk stress levels of 250 and 280 MPa.

Figure 10. *Equivalent plastic strain contour plots of the Voronoi partition region for a homogenous model and inhomogeneous models at different bulk stress levels.*

4.2 Lifetime estimation

This section presents the results of the fretting fatigue lifetime estimation conducted using the CDM + TCD methodology outlined in section 3.1. Before the lifetime prediction study could have been conducted, the CDM model had to be calibrated and the value of the TCD had to be established. The calibration of the CDM model is achieved by finding the two material parameters m and σ_r, and since the fully reversed loading condition is studied, σ_m in Equation (7) is equal to 0 and σ_r = σ_0. The two material parameters can be determined using plane fatigue data of the same material. By fitting a power law curve with the fatigue data an equation describing the fatigue behaviour of the material is generated which has the following general form:

$$\sigma_a = \sigma_f'(N)^k, \tag{13}$$

where N is the number of fatigue cycles which lead to failure at a stress value σ_a, while σ_f' and k are material constants. Converting Equation (10) in order for it to resemble Equation (13) leads to the following formula:

$$\sigma_a = \frac{\sigma_r}{(1+m)^{\frac{1}{m}}} N_f^{-\frac{1}{m}}, \tag{14}$$

which can be readily compared with Equation (13) in order to obtain the two material parameters m and σ_r:

$$-\frac{1}{m} = k, \frac{\sigma_r}{(1+m)^{1+m}} = \sigma_f' \tag{15}$$

In this research the fatigue data of S45C steel from the work by Tanaka et al. [59] is used, which results in the m value equal 14.7 to and the σ_r value equal to 821. Those values are used in Equation (10), along with the averaged in-plane principal stress in the critical grain, extracted from the FE model, to generate the fretting fatigue lifetime estimation. As for the critical distance L, necessary for the determination of the critical grain below the contact surface for the stress extraction, it is calculated using Equation (11) and the material constants taken from [51], where ΔK_{th} is reported to be 4 $\left(MPa \times m^{1/2}\right)$ and $\Delta\sigma_o$ is equal to 250 (MPa). Those values give L = 81.4 µm and so $L/2$ = 40.7 µm. The same value of $L/2$ is used in the crack propagation study.

The results of the fretting fatigue lifetime estimation are plotted in Figure 11. Figure 11 (a) displays the results obtained based on pure elastic simulations in function of bulk stress amplitude, compared with experimental results reported in [51]. Figure 11 (b) shows the results based on elasto-plastic simulations for both homogeneous and inhomogeneous models, also compared with the same set of experimental data. In case of the elastic simulations, there is a significant scatter in the predicted lifetimes. At the same bulk stress level, the lifetimes cover a range of up to two orders of magnitude and the total range of predictions varies from 10^3 to 10^8. At higher bulk stress levels, the predictions match the experimental results well as the experimental data points lie within the ranges generated by scatter in the predictions. On the other hand, at lower load levels (210 and 180 MPa), the predictions clearly overestimate the lifetimes. Moving on to the prediction results based on the elasto-plastic simulations, the range of the obtained results is much narrower as all data points fit in the range from 10^4 to 10^6 cycles. The lifetimes at different bulk stress levels also display reduced scatter with the maximum being just above one order of magnitude. The lifetime estimation obtained based on the elasto-plastic homogenous model lies within the scatter generated by the inhomogeneous model predictions.

It is also important to point out that, in contrast to the elastic simulations, the estimations at lower bulk stress levels underestimate the lifetimes. The difference in lifetimes may be attributed to the difference in stress distributions between the two models. The elastic model exhibits elevated stress concentrations at the contact interface that diminish quickly below the contact edge in the Voronoi partition region. In contrast, the elasto-plastic model displays reduced stress concentrations, but the decline is less significant, and stress levels beneath the contact surface are higher than in the elastic model. This means that the elasto-plastic model is safer to use as it will not overestimate the fretting fatigue lives of affected components which could lead to a failure during operation. In Figure 12 (a) the same prediction results as in Figure 11 (b) are plotted, but with the maximum von Mises stress in the critical grain on the y axis. Using this graph design curves of the material are generated, denoting the probability of failure for different stress levels.

Finally, obtained fretting fatigue lifetime estimations were fitted to a three-parameter Weibull distribution and the results of the analysis are shown in Figure 12 b). The y axis of the graph is the probability of failure while the x axis is a normalized parameter V which can be obtained using the following equation:

$$V = (lnN - B)(ln\sigma_v - C) \tag{16}$$

where N is the number of cycles to failure, σ_v is the Von Mises stress, B and C are calibrated Weibull model parameters: threshold parameter for lifetime and threshold parameter for stress level. Using the normalized value V makes it possible to compare specimen subjected to different stress levels and include all data points on a single Weibull plot. The normalization criterion is the percentile based normalization which takes advantage of the compatibility condition between $\Delta\sigma$ and N_f. This condition originates from the fact that the mean and variance of the N_f depend on $\Delta\sigma$, and in the same way the mean and variance of $\Delta\sigma$ depend on N_f. Detailed description and derivation of the applied model can be found in [60]. Based on the obtained graph one can see that for small changes in V, the probability of failure increases significantly. This means that for small changes in the von Mises stress or a small increase in the number of elapsed fretting fatigue cycle, the likelihood of failure becomes much higher.

Not included in this investigation is the effect of wear, which can have an impact on the lifetime of components subjected to fretting fatigue, depending on the slip-stick conditions. Past researches [24,61] show that under partial slip conditions there is relatively little wear and fretting damage increases, with a high risk of cracking at the contact edges due to stress concentrations. On the other hand, under gross slip conditions, wear suppresses early crack initiation and transforms the surface, which results in stress redistribution and increased fretting fatigue lifetimes. Pinto et al. [10] observed this phenomenon in their lifetime predictions, where inclusion of wear effects in the simulation increased the lifetime at higher bulk stress levels, at which gross slip occurred throughout larger portion of the fatigue cycle. At lower bulk stress levels, where stick-slip conditions dominate, the lifetime decreased, but in both cases the changes were relatively minor. In case of the presented model, inclusion of wear is believed to have a similar, but even less pronounced effect on the lifetime predictions, because the stress values used in the TCD + CDM approach are extracted from below the contact surface.

Figure 11. *SN curves showing the number of cycles to failure (N_f) plotted against bulk stress amplitude ($\Delta\sigma$) for a purely elastic models (a) and elasto-plastic models (b).*

Figure 12. *SN curve curves showing the number of cycles to failure (N_f) plotted against maximum von Mises stress in the critical grain ($\sigma_{von\ Mises}$) for elasto-plastic models (a) and cumulative distribution function of the lifetime estimations obtained based on the Weibull model (b).*

4.3 Crack propagation path

The results of the crack propagation simulations are shown in Figure 13. Each figure displays the position of the crack tip for three different simulations with the same bulk stress levels but different Voronoi partition regions. Those simulated crack paths are compared to experimental crack propagation path, obtained for a bulk stress level of 300 MPa, taken from [51]. Simulated crack paths show good agreement with the experimental results, the overall propagation direction is towards the centre of contact and only small deviations are present at higher bulk stress levels. Better match between the reference and the crack paths obtained at 180 MPa, rather than the paths obtained at 300 MPa could be explained by the effect of microstructure randomness on the crack propagation direction.

Presented results show that with the increasing bulk stress the impact of microstructural inhomogeneity on crack path increases. At 180 MPa very little scatter in crack propagation angle at different crack propagation increments is observed. As shown in Figure 14. (a) – (c), the crack passes through grains with different elasto-plastic properties but the crack propagation angle stays in the range between 100° and 111°. At 210 MPa the deflections in crack path become more significant. They start at the depth of 60 µm and occur when crack approaches areas with high differences in the material properties of the grains which positioned next to each other in the crack propagation direction, as can be seen in Figure 14. (d) and (e). Similar behaviour can be observed for the simulations performed at 250 MPa, but the crack paths start to deflect earlier, at the depth of 40 µm. All simulated cracks follow similar path close to the surface, but only the path for the simulation IH-FFM18-250 was successfully run past the depth of 100 µm and is shown in Figure 14. (f), the other two failed to reach convergence earlier, possibly due to difficult to resolve high stress concentrations around the crack tip.

The scatter in crack paths caused by microstructure randomness is most clearly visible at the bulk stress of 300 MPa. The simulations IH-F0FM16-300 and IH-FFM55-300 follow very similar crack path, possibly due to the fact that in both cases the propagation occurs through high stress grains, as shown in Figure 14 (h) and (i). Only at the depth of 140 µm, the crack path in the IH-FFM16-300 simulation deviates slightly as it encounters a region of high difference between grain properties, with strongest and weakest grains next to each other and the crack path moving from a strong grain to a weak one. Crack path in the simulation IH-FFM03-300 deflects to the right early, possibly due to alternating strong and weak grains in the propagation path. Despite that, all three simulated paths meet close to the bottom edge of the Voronoi partition region, as shown in Figure 14 (d), which is likely caused by the proximity to the uniform test specimen.

Figure 13. *The position of the crack tip in the conducted simulations at different bulk stress levels: (a) 180 MPa, (b) 210 MPa, (c) 250 MPa and (d) 300 MPa, compared with the experimental crack path taken from* [51].

Figure 14. *Simulated crack propagation paths which progressed past the midpoint of the Voronoi partition region.*

Figure 15 depicts the comparison between the equivalent plastic strain distributions for two models, with and without the propagated crack. In Figure 15 (a) significant plastic strain near the contact interface can be observed and the plastic strain in the weak grains reaches halfway deep into the Voronoi partition region. When the bulk stress is increased to 300 MPa, the equivalent plastic strain near the top edge of the Voronoi partition region extends beyond the contact interface as shown in Figure 15 (c). Moreover, plasticized grains reach the bottom edge of the Voronoi region and the maximum equivalent plastic strain increases to 0.045 from 0.028. When the crack is introduced, a significant yielded zone can be observed around the crack tip, as shown in Figure 15 (b) and (d). Additionally, the maximum values of the equivalent plastic strain are also significantly higher when the crack is introduced, for the simulation conducted at the maximum bulk stress of 300 MPa the maximum PEEQ value is more than two times higher.

Figure 15. *The equivalent plastic strain contour plots of the Voronoi partition region for two bulk stress levels of 180 MPa and 300 MPa, plots (a) and c) depict the results without a propagated crack, while plots (b) and (d) show the results with a propagated crack.*

The crack propagation simulations, performed with the penalty friction formulation and a coefficient of friction (COF) of 0.1, resulted in a majority of the simulations not reaching the midpoint of the Voronoi partition region. This was attributed to the high stress concentrations around the crack tip, which were challenging to resolve and resulted in non-convergence of the simulations. Only in the case of simulations performed at 300 MPa did all three simulations progress past the halfway point. The primary difference between these simulations and those performed with frictionless contact behaviour was the increased stress values around the crack tip, with a varying magnitude between simulations. In the last successfully completed step, in the model IH-FFM55-300, the maximum von Mises stress value was only 1.7% higher in the simulation with specified friction, whereas in model IH-FFM55-300, that increase was equal to 20%. Despite these potential differences in stress values, the effect of the specified tangential friction on the predicted crack paths was negligible, as demonstrated in Figure 16. The simulated crack paths for both cases were nearly identical, with small deviations observed at lower depths of the Voronoi partition element, indicating that the method used to predict crack propagation direction was not impacted by the stress concentrations around the crack tip.

Figure 16. *The position of the crack tip in the conducted simulations with frictionless and penalty friction tangential contact, at the bulk stress level of 300 MPa, compared with the experimental crack path taken from* [51].

5. Conclusion

The effect of microstructural inhomogeneity on the fretting fatigue response of the S45C steel was investigated. Fretting fatigue model of the bridge-type contact was created and the microstructural grains of the specimen material were modelled using FEM and Voronoi tessellation. Each grain was randomly assigned with one of the pre-prepared elasto-plastic material properties in order to simulate the microstructure randomness. In total 58 simulations were successfully conducted and based on the obtained results a lifetime estimation study was performed using a CDM based methodology combined with the principle of TCD. The goal was to evaluate the effect of variance in grain distribution and properties on the fretting fatigue lifetime and capture the scatter characteristic of practical experiments. Moreover, XFEM was used to investigate the effect microstructural inhomogeneity has on crack propagation paths under fretting fatigue conditions.

Obtained results show that the microstructural inhomogeneity can have a significant impact on the distribution of contact stresses in fretting fatigue. In the analysed cases peak shear stress value can be up to 23% higher in the inhomogeneous model compared to a homogenous one. The change in the peak tangential stress, observed at the contact edge, can also be considerable. Based on the simulation results the stress values are up to 15.4% lower or up to 17.2% higher compared to the homogenous model for the studied cases. This is especially important since tangential stresses at the contact edge have been shown to have a significant impact on the crack initiation process, and by extension the lifetime of affected components. Moreover, the contact width changes based on the microstructural inhomogeneity as well, which leads to different likely crack initiation points.

As for the results of the lifetime estimation, the predicted lifetimes of elasto-plastic, inhomogeneous models show a scatter of one order of magnitude for a given bulk stress level when compared to reference experimental results. The scatter bands obtained that way are centred around the experimental data points for higher bulk stress levels and lie below those data points for lower bulk stress levels. Obtained predictions simulate the scatter often observed in experimental results well and have been used to propose a design curve for the S45C steel. Furthermore, the relationship between the probability of failure, fretting fatigue cycles, and von Mises stress was examined using Weibull statistics. The analysis demonstrated that even a slight increase in these parameters significantly enhances the likelihood of failure, and highlighting the potential value of this approach in the design process.

On the other hand, it is important to point out that the proposed modelling technique considers only the effect of microstructure randomness on fretting fatigue lifetime, but in laboratory test there are multiple other sources of scatter. Those include: surface quality, presence of subsurface imperfections, accuracy of the testing equipment, laboratory environment and the skill of laboratory technicians. This should be taken into account when interpreting the results and warrants further study into the effect of microstructural inhomogeneity on fretting fatigue response.

The results of the crack propagation study highlight the ability of the proposed model to simulate the scatter in crack paths due to microstructural inhomogeneity. Predicted crack paths propagate towards the centre of contact, similar to the reference experimental results. On the other hand, clear scatter in the paths can be observed, the degree of which increases with increasing bulk stress levels. Observed deflections occur when the propagating crack approaches grains with large differences between their elasto-plastic properties but seems to propagate more smoothly through grains with similar strength. Further studies could investigate how the range of applied material properties affects the fretting fatigue lifetime predictions. Moreover, a statistical approach could be applied to simulate the range of grain properties using normal distribution, which would bring the model closer to a real life situation. Future investigations could also incorporate the presence of the grain boundaries in the FE model in order to evaluate their effect on crack propagation paths, which could offer additional insight into the crack propagation behaviour under fretting fatigue conditions. Another possible research direction could focus on the effect of higher COF values on the predicted lifetimes and crack paths. Nonetheless, the developed model and performed study provide valuable insight into the effect of microstructural inhomogeneity on fretting fatigue response and highlight the importance of further research into this field.

Declaration of Competing Interests

The authors declare that they have no known competing financial interests or personal relationships that could have appeared to influence the work reported in this paper.

Data availability

Data will be made available on request.

References

[1] Jiménez-Peña C, H. Talemi R, Rossi B, Debruyne D. Investigations on the fretting fatigue failure mechanism of bolted joints in high strength steel subjected to different levels of pre-tension. Tribol Int 2017;108:128–40. https://doi.org/10.1016/j.triboint.2016.11.014.

[2] Venugopal Poovakaud V, Jiménez-Peña C, Talemi R, Coppieters S, Debruyne D. Assessment of fretting fatigue in high strength steel bolted connections with simplified Fe modelling techniques. Tribol Int 2020;143. https://doi.org/10.1016/j.triboint.2019.106083.

[3] Matos IM, Rocha PHC, Kalombo RB, Veloso LACM, Araújo JA, Castro FC. Fretting fatigue of 6201 aluminum alloy wires of overhead conductors. Int J Fatigue 2020;141:105884. https://doi.org/10.1016/j.ijfatigue.2020.105884.

[4] Erena D, Vázquez J, Navarro C, Talemi R. Numerical study on the influence of artificial internal stress relief groove on fretting fatigue in a shrink-fitted assembly. Tribol Int 2020;151. https://doi.org/10.1016/j.triboint.2020.106443.

[5] Glodek G, Talemi R. An applied approach for estimating fretting fatigue lifetime of dovetail joints using coupon scale test data. Theor Appl Fract Mech 2022;121:103455. https://doi.org/10.1016/J.TAFMEC.2022.103455.

[6] Toler BF, Coutu RA, McBride JW. A review of micro-contact physics for microelectromechanical systems (MEMS) metal contact switches. J Micromechanics Microengineering 2013;23:103001. https://doi.org/10.1088/0960-1317/23/10/103001.

[7] NTSB. Left Engine Failure and Subsequent Depressurization, Southwest Airlines Flight 1380, Boeing 737-7H4, N772SW. 2018.

[8] Talemi RH. Numerical measures of non-proportionality degree in incomplete contact subjected to fretting fatigue loading. Theor Appl Fract Mech 2017;90:33–42. https://doi.org/https://doi.org/10.1016/j.tafmec.2017.02.010.

[9] Talemi R. A numerical study on effects of randomly distributed subsurface hydrogen pores on fretting fatigue behaviour of aluminium AlSi10Mg. Tribol Int 2020;142:105997. https://doi.org/10.1016/j.triboint.2019.105997.

[10] Pinto AL, Araújo JA, Talemi R. Effects of fretting wear process on fatigue crack propagation and life assessment. Tribol Int 2021;156:106787. https://doi.org/10.1016/j.triboint.2020.106787.

[11] Bhadeshia H, Honeycombe R. Steels: microstructure and properties. 4th ed. Butterworth-Heinemann; 2017.

[12] Nesládek M, Španiel M, Jurenka J, Růžička J, Kuželka J. Fretting fatigue - Experimental and numerical approaches. Int J Fatigue 2012;44:61–73. https://doi.org/10.1016/j.ijfatigue.2012.05.015.

[13] Wang J, Xu H, Su T, Zhang Y, Guo Z, Mao H, et al. Fretting fatigue experiment and analysis of AlSi9Cu2Mg alloy. Materials (Basel) 2016;9:1–13.

https://doi.org/10.3390/ma9120984.

[14] Venkatesh TA, Conner BP, Lee CS, Giannakopoulos AE, Lindley TC, Suresh S. An Experimental Investigation of Fretting Fatigue in Ti-6Al-4V : the Role of Contact Conditions and Microstructure 2001;32:1131–1146. https://doi.org/10.1007/s11661-001-0124-8.

[15] Lütjering G. Influence of processing on microstructure and mechanical properties of (α+ β) titanium alloys. Mater Sci Eng A 1998;243:32–45.

[16] Mall S, Namjoshi SA, Porter WJ. Effects of microstructure on fretting fatigue crack ititiation behavior of Ti-6Al-4V. Mater Sci Eng A 2004;383:334–40. https://doi.org/10.1016/j.msea.2004.05.019.

[17] Hong J, Kim I, Park C, Kim E. Microstructural effects on the fretting wear of Inconel 690 steam generator tube 2005;259:349–55. https://doi.org/10.1016/j.wear.2004.12.007.

[18] Mall S, Kim H, Saladin EC, Porter WJ. Effects of microstructure on fretting fatigue behavior of IN100 2010;527:1453–60. https://doi.org/10.1016/j.msea.2009.10.068.

[19] Goh C, Wallace JM, Neu RW, Mcdowell DL. Polycrystal plasticity simulations of fretting fatigue 2001;23:423–35.

[20] Goh C, Mcdowell DL, Neu RW. Characteristics of plastic deformation field in polycrystalline fretting contacts 2003;25:1047–58. https://doi.org/10.1016/j.ijfatigue.2003.08.004.

[21] Goh C, Neu RW, Mcdowell DL. Crystallographic plasticity in fretting of Ti – 6AL – 4V 2003;19:1627–50.

[22] Dick T, Cailletaud G. Fretting modelling with a crystal plasticity model of Ti6Al4V 2006;38:113–25. https://doi.org/10.1016/j.commatsci.2006.01.015.

[23] Dick T, Basseville S, Cailletaud G. Fatigue modelling in fretting contact with a crystal plasticity model 2008;43:36–42. https://doi.org/10.1016/j.commatsci.2007.07.055.

[24] Mccarthy OJ, Mcgarry JP, Leen SB. Micro-mechanical modelling of fretting fatigue crack initiation and wear in Ti – 6Al – 4V. Int J Fatigue 2014;62:180–93. https://doi.org/10.1016/j.ijfatigue.2013.04.019.

[25] Ren C, Zhang X, Ji H, Wang H. Damage evolution and failure mechanism induced by microstructural inhomogeneity in bainite steel. Eng Fail Anal 2021;128:105602. https://doi.org/10.1016/j.engfailanal.2021.105602.

[26] Sun L, Thomas MJ, Wynne BP, Palmiere EJ, Mingard KP. Mapping microstructure inhomogeneity using electron backscatter diffraction in 316L stainless steel subjected to hot plane strain compression tests 2010;26:1477–86. https://doi.org/10.1179/026708310X12688283410280.

[27] Das A, Chekhonin P, Altstadt E, Bergner F, Heintze C, Lindau R. Microstructural characterization of inhomogeneity in 9Cr ODS EUROFER steel. J Nucl Mater 2020;533:152083. https://doi.org/10.1016/j.jnucmat.2020.152083.

[28] Mayeur JR, Mcdowell DL, Neu RW. Crystal plasticity simulations of fretting of Ti-6Al-4V

in partial slip regime considering effects of texture 2008;41:356–65. https://doi.org/10.1016/j.commatsci.2007.04.020.

[29] Zhang MÃ, Mcdowell DL, Neu RW. Microstructure sensitivity of fretting fatigue based on computational crystal plasticity. Tribol Int 2009;42:1286–96. https://doi.org/10.1016/j.triboint.2009.04.036.

[30] Mccarthy OJ, Mcgarry JP, Leen SB. The effect of grain orientation on fretting fatigue plasticity and life prediction. Tribiology Int 2014;76:100–15. https://doi.org/10.1016/j.triboint.2013.09.023.

[31] Ashton PJ, Harte AM, Leen SB. Statistical grain size effects in fretting crack initiation. Tribol Int 2017;108:75–86. https://doi.org/10.1016/j.triboint.2016.09.022.

[32] Ashton PJ, Harte AM, Leen SB. A strain-gradient, crystal plasticity model for microstructure-sensitive fretting crack initiation in ferritic-pearlitic steel for flexible marine risers. Int J Fatigue 2018;111:81–92. https://doi.org/10.1016/j.ijfatigue.2018.01.028.

[33] McDowell DL, Dunne FPE. Microstructure-sensitive computational modeling of fatigue crack formation. Int J Fatigue 2010;32:1521–42. https://doi.org/10.1016/j.ijfatigue.2010.01.003.

[34] Sangid MD. The physics of fatigue crack initiation. Int J Fatigue 2013;57:58–72. https://doi.org/10.1016/j.ijfatigue.2012.10.009.

[35] Sweeney CA, Vorster W, Leen SB, Sakurada E, Mchugh PE, Dunne FPE. Journal of the Mechanics and Physics of Solids The role of elastic anisotropy , length scale and crystallographic slip in fatigue crack nucleation. J Mech Phys Solids 2013;61:1224–40. https://doi.org/10.1016/j.jmps.2013.01.001.

[36] Slack TS, Leonard BD, Sadeghi F. Estimating life scatter in fretting fatigue crack initiation. Tribol Trans 2013;56:531–5. https://doi.org/10.1080/10402004.2013.766829.

[37] Walvekar AA, Leonard BD, Sadeghi F, Jalalahmadi B, Bolander N. An experimental study and fatigue damage model for fretting fatigue. Tribol Int 2014;79:183–96. https://doi.org/10.1016/j.triboint.2014.06.006.

[38] Kachanov L. Time of the Rupture Process under Creep Conditions. Izv Akad Nauk SSSR Otd Teckhnicheskikh 1958;8:26–31.

[39] Lemaitre J. Evaluation of dissipation and damage in metals. Proc. ICM Kyoto, vol. 1, 1971.

[40] Lemaitre J, Chaboche JL. A non-linear model of creep-fatigue damage cumulation and interaction(for hot metallic structures). Mech Visco-Elastic Media Bodies 1975.

[41] Lemaitre J. A Continuous Damage Mechanics Model for Ductile Fracture. J Eng Mater Technol 1985;107:83–9. https://doi.org/10.1115/1.3225775.

[42] Bhattacharya B, Ellingwood B. Continuum damage mechanics analysis of fatigue crack initiation. Int J Fatigue 1998;20:631–9.

[43] Namjoshi SA, Mall S, Jain VK, Jin O. Fretting fatigue crack initiation mechanism in Ti-6Al-4V. Fatigue Fract Eng Mater Struct 2002;25:955–64. https://doi.org/10.1046/j.1460-2695.2002.00549.x.

[44] Hutson AL, Neslen C, Nicholas T. Characterization of fretting fatigue crack initiation processes in CR Ti-6Al-4V. Tribol Int 2003;36:133–43. https://doi.org/10.1016/S0301-679X(02)00138-X.

[45] Szolwinski MP, Farris TN. Mechanics of fretting fatigue crack formation. Wear 1996;198:93–107. https://doi.org/10.1016/0043-1648(96)06937-2.

[46] Nowell D, Dini D. Stress gradient effects in fretting fatigue. Tribol Int 2003;36:71–8. https://doi.org/10.1016/S0301-679X(02)00134-2.

[47] Araújo JA, Nowell D. The effect of rapidly varying contact stress fields on fretting fatigue. Int J Fatigue 2002;24:763–75. https://doi.org/https://doi.org/10.1016/S0142-1123(01)00191-8.

[48] Sunde SL, Haugen B, Berto F. Experimental and numerical fretting fatigue using a new test fixture. Int J Fatigue 2021;143. https://doi.org/10.1016/j.ijfatigue.2020.106011.

[49] Hu C, Wei D, Wang Y, Shi L. Experimental and numerical study of fretting fatigue in dovetail assembly using a total life prediction model. Eng Fract Mech 2019;205:301–18. https://doi.org/10.1016/j.engfracmech.2018.08.001.

[50] Taylor D. The theory of critical distances. Eng Fract Mech 2008;75:1696–705. https://doi.org/10.1016/j.engfracmech.2007.04.007.

[51] Noraphaiphipaksa N, Manonukul A, Kanchanomai C. Fretting fatigue with cylindrical-on-flat contact: Crack nucleation, crack path and fatigue life. Materials (Basel) 2017;10. https://doi.org/10.3390/ma10020155.

[52] Nguyen VP, Nguyen NPL, Dang TN. Improvement for Microstructure of Severely Deformed JIS S45C Steel after Rolling Process. Appl Mech Mater 2019;889:148–54. https://doi.org/10.4028/www.scientific.net/amm.889.148.

[53] Kamaya M. Ramberg-Osgood type stress-strain curve estimation using yield and ultimate strengths for failure assessments. Int J Press Vessel Pip 2014;137:1–12. https://doi.org/10.1016/j.ijpvp.2015.04.001.

[54] Qiu H, Ueji R, Kimura Y, Inoue T. Heterogeneous distribution of microstrain evolved during tensile deformation of polycrystalline plain low carbon steel. Metals (Basel) 2020;10:1–11. https://doi.org/10.3390/met10060774.

[55] Anjum Z, Qayyum F, Khushnood S, Ahmed S, Shah M. Prediction of non-propagating fretting fatigue cracks in Ti6Al4V sheet tested under pin-in-dovetail configuration: Experimentation and numerical simulation. Mater Des 2015;87:750–8. https://doi.org/10.1016/j.matdes.2015.08.070.

[56] Williams ML. Stress Singularities Resulting From Various Boundary Conditions in Angular Corners of Plates in Extension. J Appl Mech Trans ASME 1952;19:526–8. https://doi.org/10.1115/1.2791085.

[57] Zak AR, Williams ML. Crack point stress singularities at a bi-material interface. J Appl Mech Trans ASME 1963;30:142–3. https://doi.org/10.1115/1.3630064.

[58] Navarro C, Vázquez J, Domínguez J. Nucleation and early crack path in fretting fatigue. Int J Fatigue 2017;100:602–10. https://doi.org/10.1016/j.ijfatigue.2016.12.028.

[59] Tanaka K, Mutoh Y, Sakoda S, Leadbeater G. Fretting Fatigue in 0.55C Spring Steel and 0.45C Carbon Steel. Fatigue Fract Eng Mater Struct 1985;8:129–42.

[60] Castillo E, Canteli AF. A Unified Statistical Methodology for Modeling Fatgiue Damage. vol. 1. 2009. https://doi.org/https://doi.org/10.1007/978-1-4020-9182-7.

[61] Basseville S, Cailletaud DMBG. 3D finite element study of the fatigue damage of Ti – 6Al – 4V in presence of fretting wear. Comput Mech 2019;64:663–83. https://doi.org/10.1007/s00466-019-01675-6.

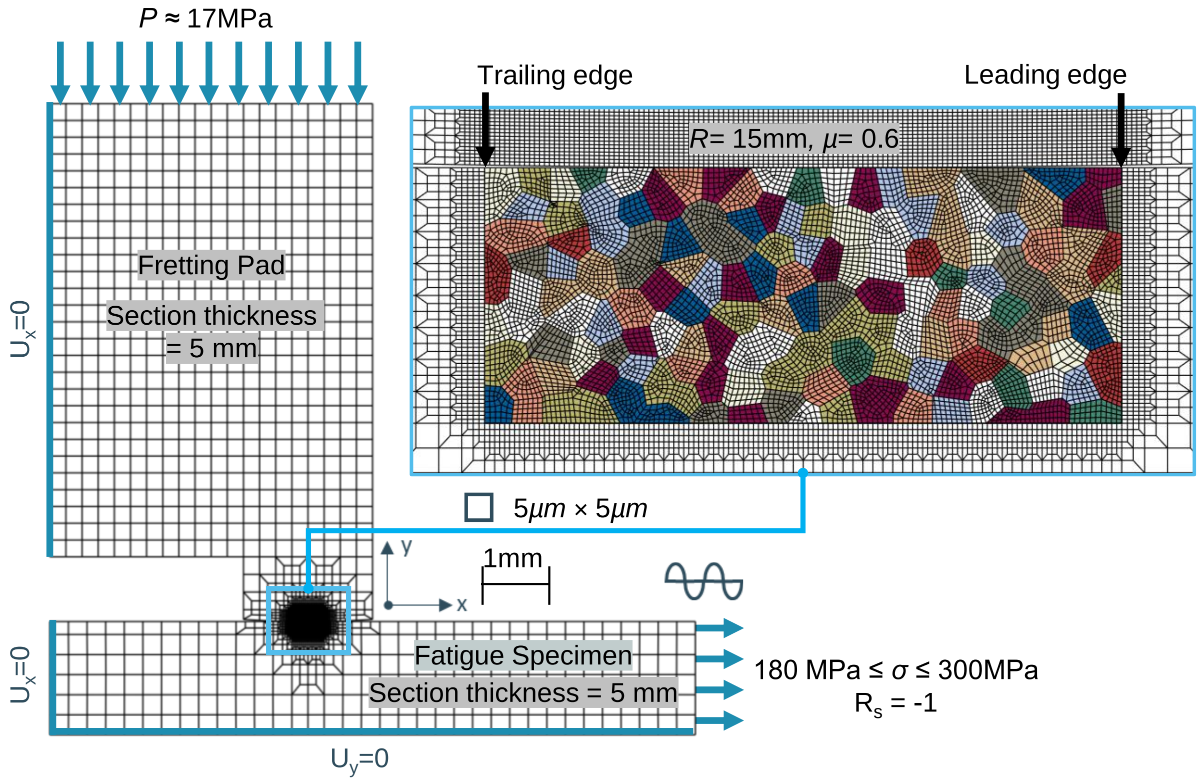

Figure 1. *The loading and boundary conditions, as well as the mesh structure of the Voronoi tessellation FE model representing the fretting fatigue testing set-up. The exact dimensions of all elements can be found in the work by Noraphaiphipaksa et al. [39].*

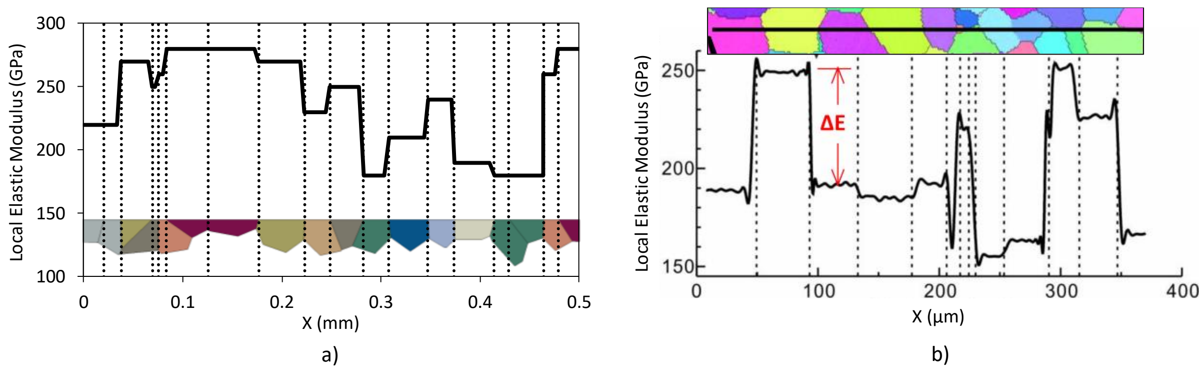

***Figure 2**. (a) The distribution of the local elastic modulus on the contact surface of the Voronoi partition region in the FE fretting fatigue model and (b) experimentally determined distribution of the local elastic modulus on the surface of a steel specimen* [54].

***Table 1**. Properties of the different material parameters assigned to the microstructural grains.*

Material	**1**	**2**	**3**	**4**	**5**	**6**	**7**	**8**	**9**	**10**	**11**
$\boldsymbol{E\ (GPa)}$	180	190	200	210	220	230	240	250	260	270	280
$\boldsymbol{\sigma_y\ (MPa)}$	352	372	392	412	432	452	472	492	512	532	552
$\boldsymbol{\sigma_{UTS}\ (MPa)}$	664	702	740	778	816	854	892	930	968	1006	1044

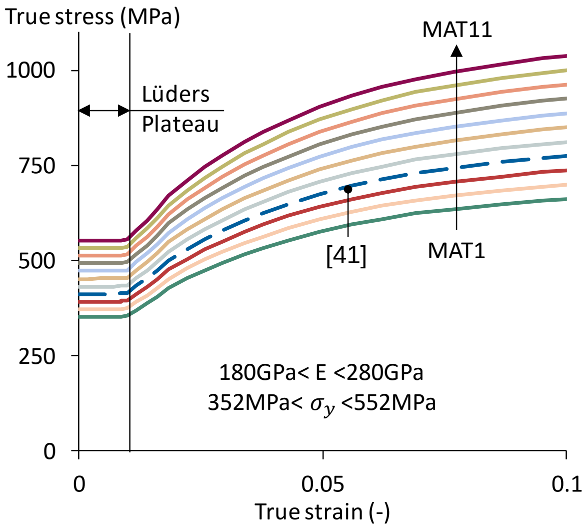

Figure 3. *Stress strain curves used to simulate the variation of mechanical properties of different grains in S45C steel.*

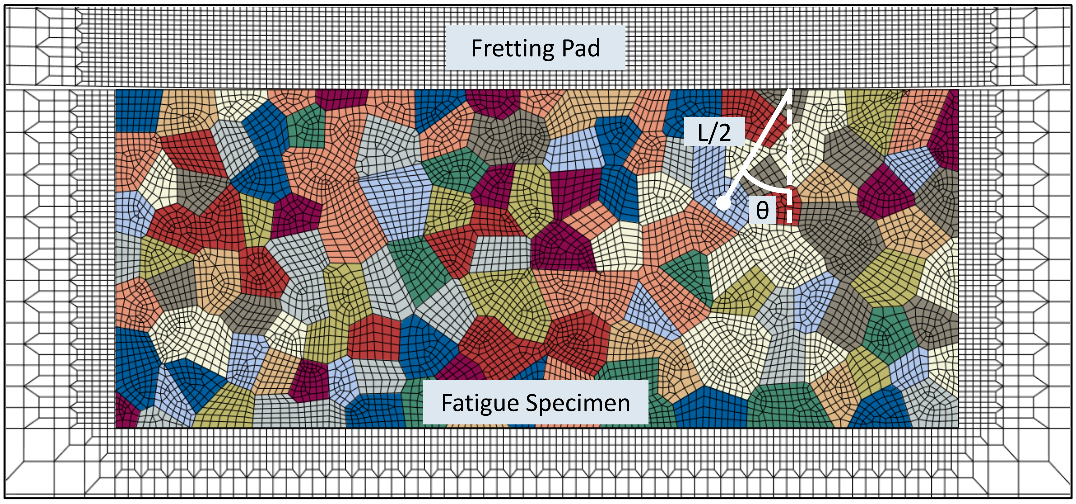

Figure 4. *Determination of the critical grain for the extraction of the damaging stress used in the lifetime estimation process.*

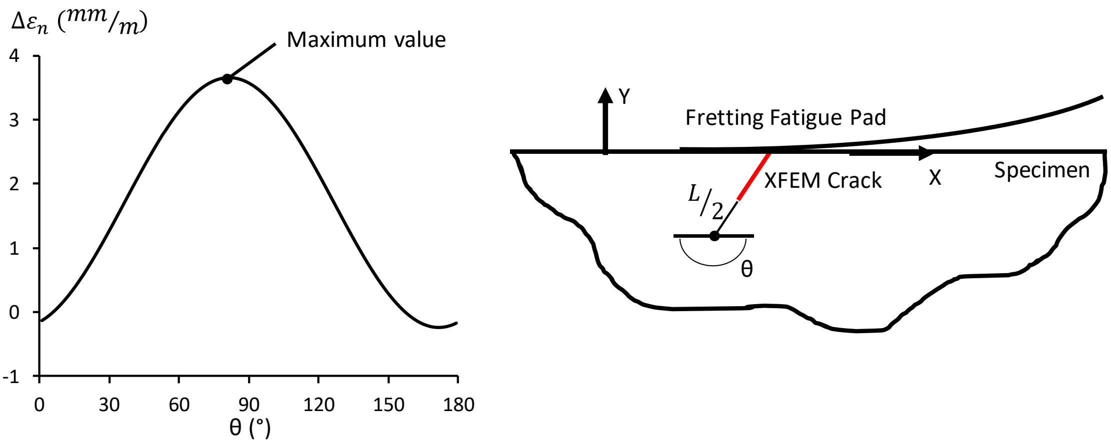

Figure 5. *Schematic representation of the methodology used for crack propagation path prediction.*

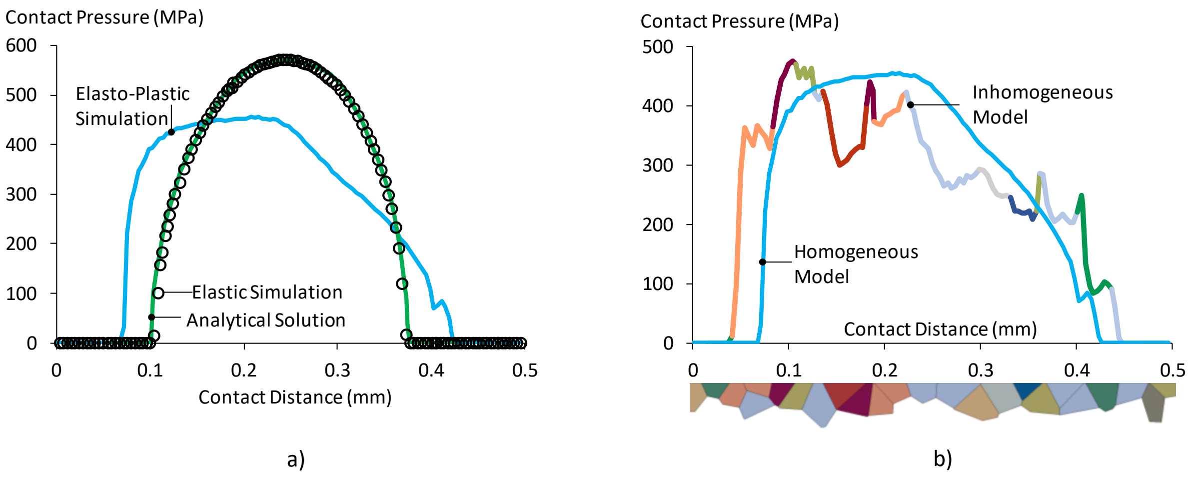

Figure 6. *Contact pressure distribution in the specimen for elastic and homogenous elasto-plastic models compared with the analytical solution (a) and contact pressure distribution in the homogenous and inhomogeneous models (b).*

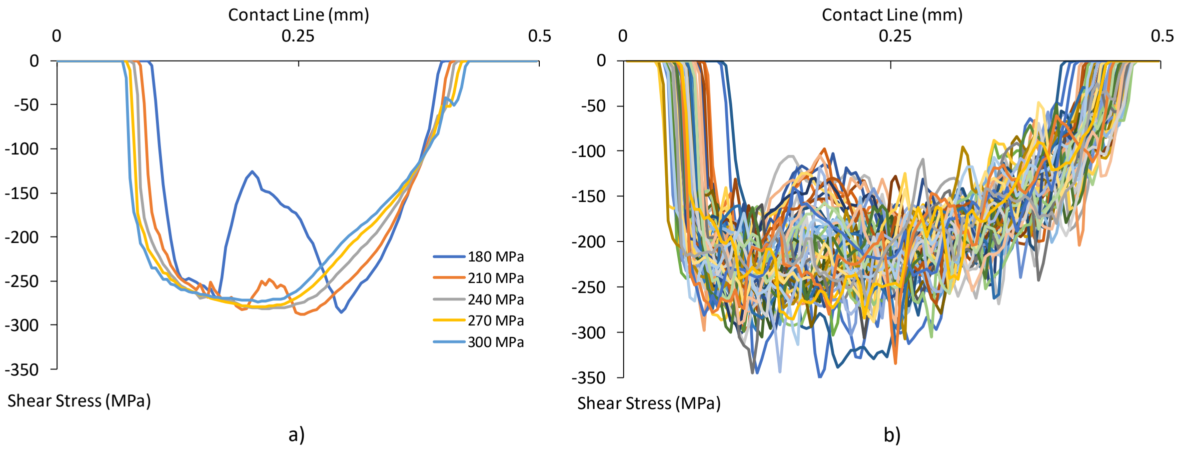

Figure 7. *Distribution of shear stress at the contact edge of the specimen, at the maximum bulk stress level, for a homogenous (a) and inhomogeneous (b) fretting fatigue models.*

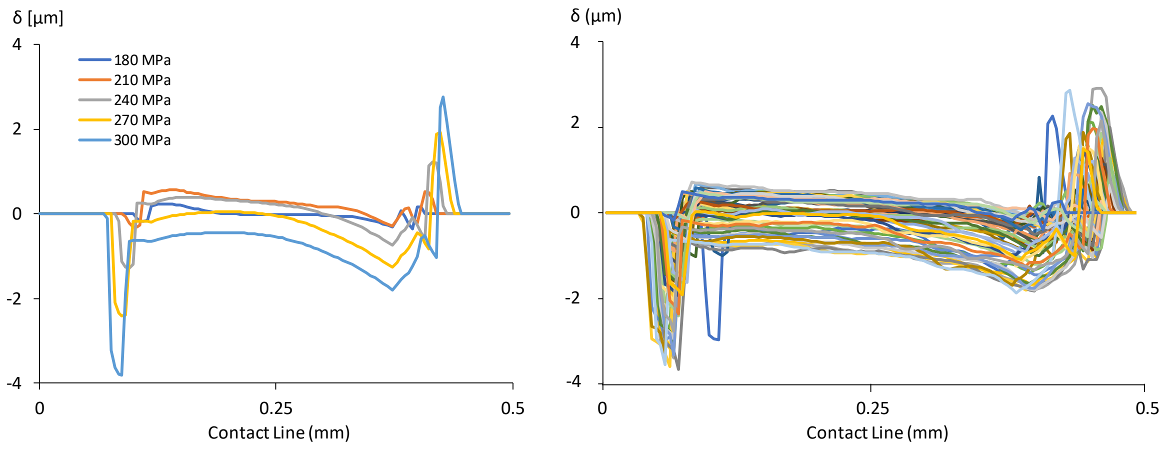

a) b)

Figure 8. *Distribution of slip amplitude at the contact interface between the specimen and the pad, at the maximum bulk stress level, for a homogenous (a) and inhomogeneous (b) fretting fatigue models.*

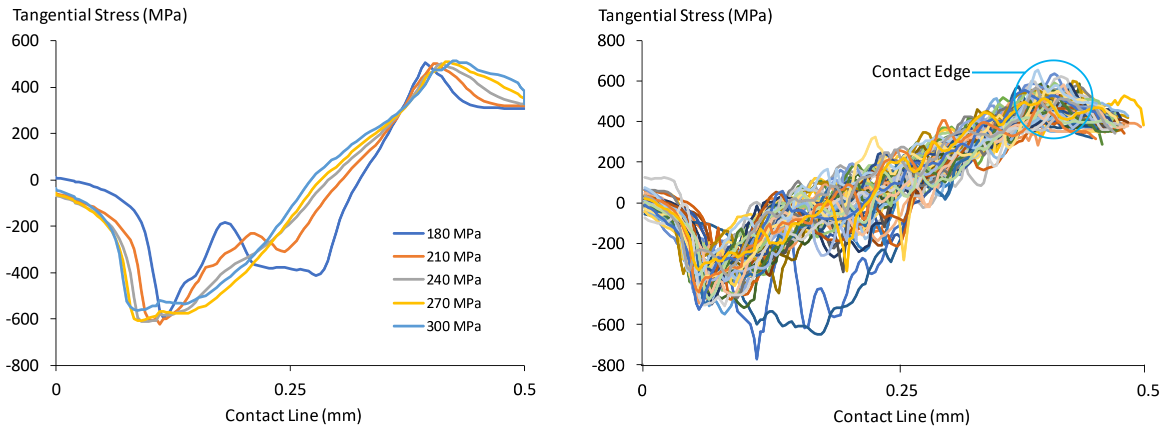

a) b)

Figure 9. *Distribution of tangential stress at the contact interface between the specimen and the pad , at the maximum bulk stress level, for a homogenous (a) and inhomogeneous (b) fretting fatigue models.*

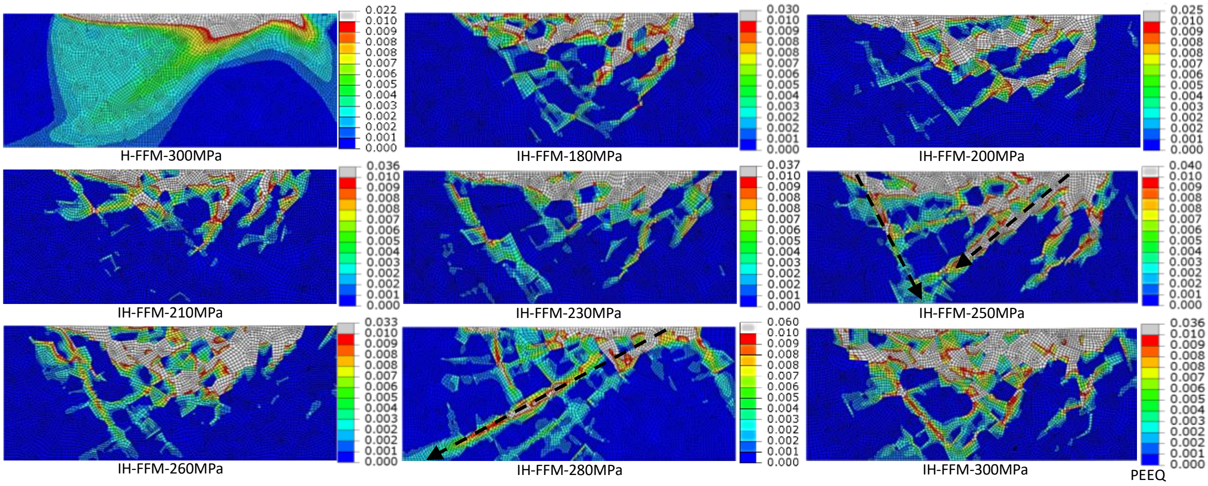

Figure 10. *Equivalent plastic strain contour plots of the Voronoi partition region for a homogenous model and inhomogeneous models at different bulk stress levels.*

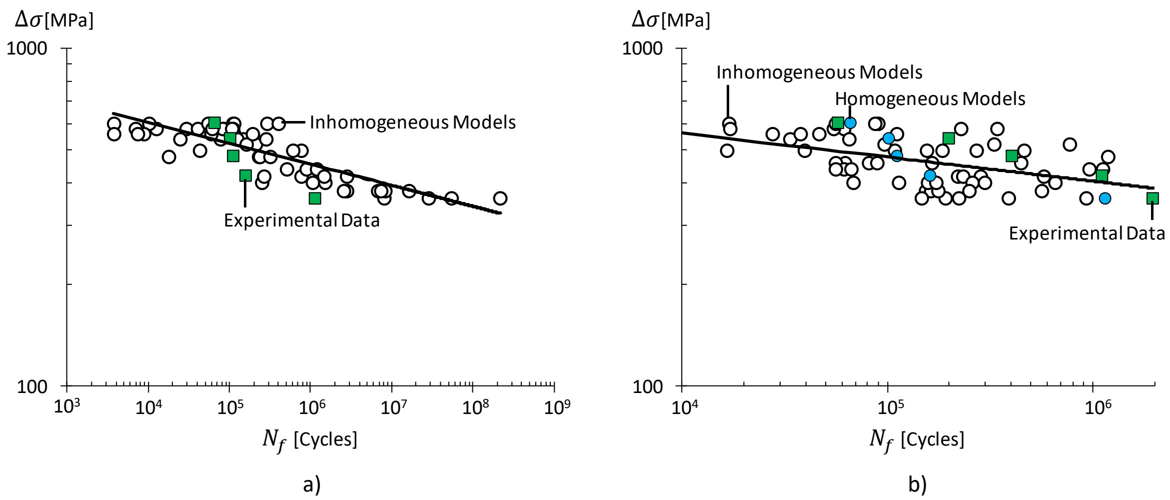

Figure 11. *SN curves showing the number of cycles to failure (N_f) plotted against bulk stress amplitude (Δσ) for a purely elastic models (a) and elasto-plastic models (b).*

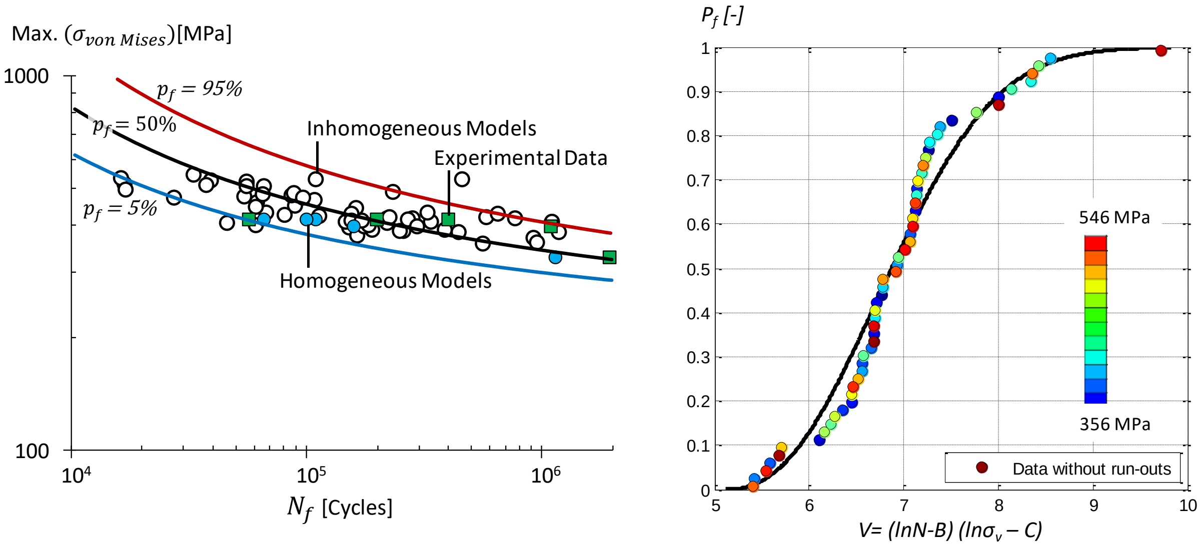

a) b)

Figure 12. *SN curve curves showing the number of cycles to failure (N_f) plotted against maximum von Mises stress in the critical grain ($\sigma_{von\ Mises}$) for elasto-plastic models (a) and cumulative distribution function of the lifetime estimations obtained based on the Weibull model.*

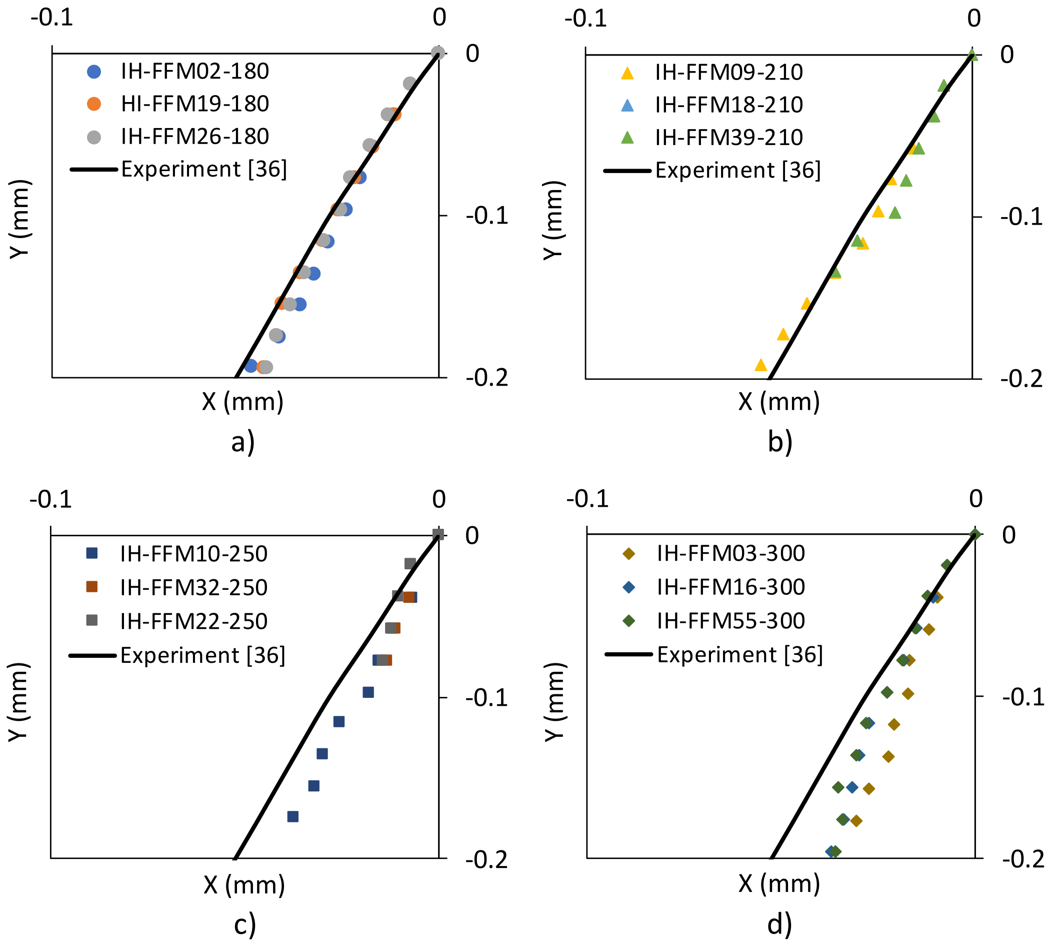

Figure 13. *The position of the crack tip in the conducted simulations at different bulk stress levels: (a) 180 MPa, (b) 210 MPa, (c) 250 MPa and (d) 300 MPa, compared with the experimental crack path taken from* [51].

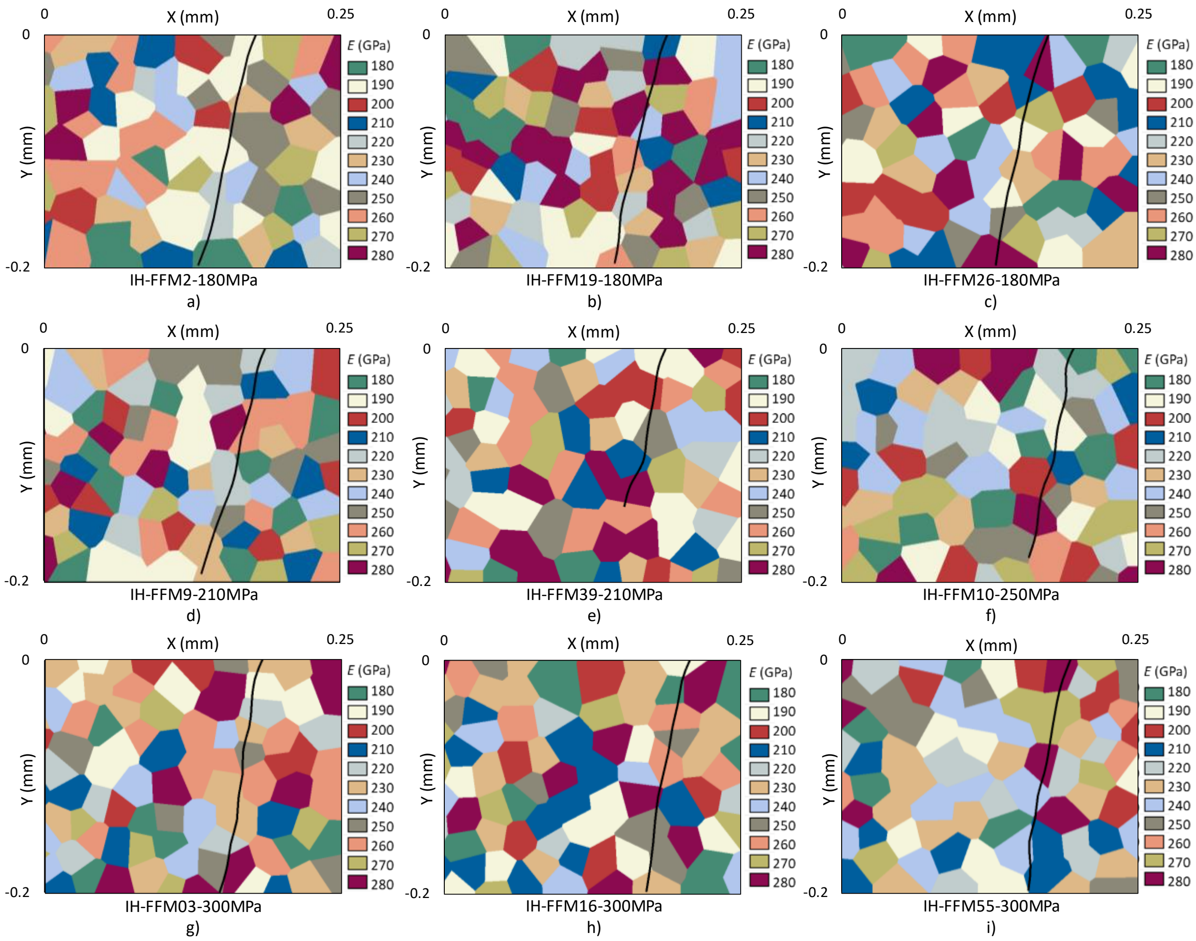

Figure 14. *Simulated crack propagation paths which progressed past the second propagation step.*

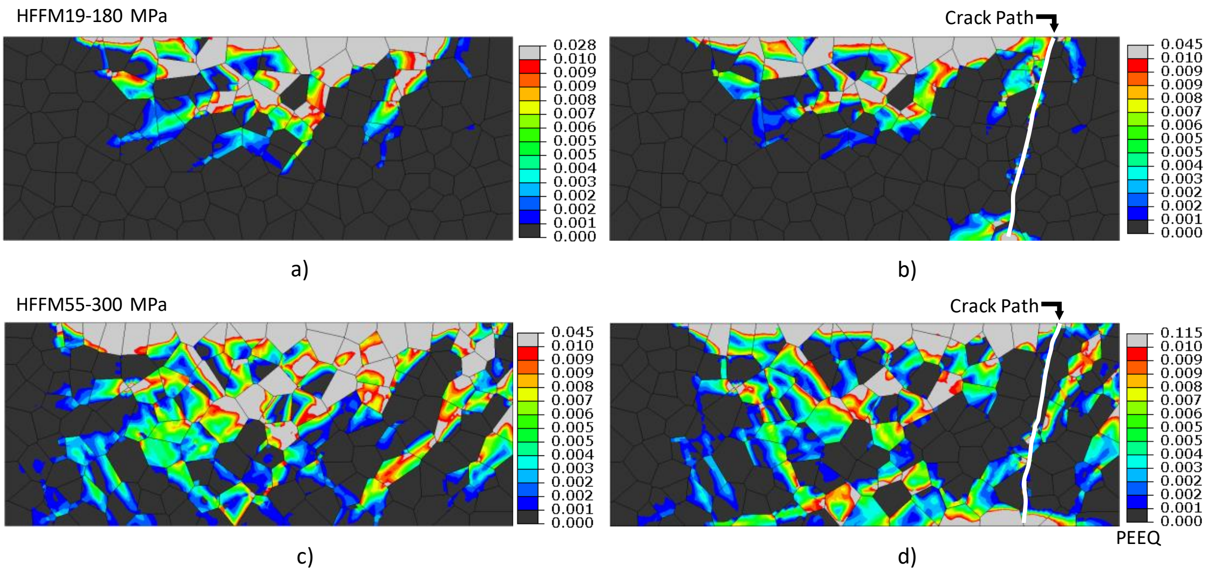

Figure 15. *The equivalent plastic strain contour plots of the Voronoi partition region for two bulk stress levels of 180 MPa and 300 MPa, plots (a) and (c) depict the results without a propagated crack, while plots (b) and (d) show the results with a propagated crack.*

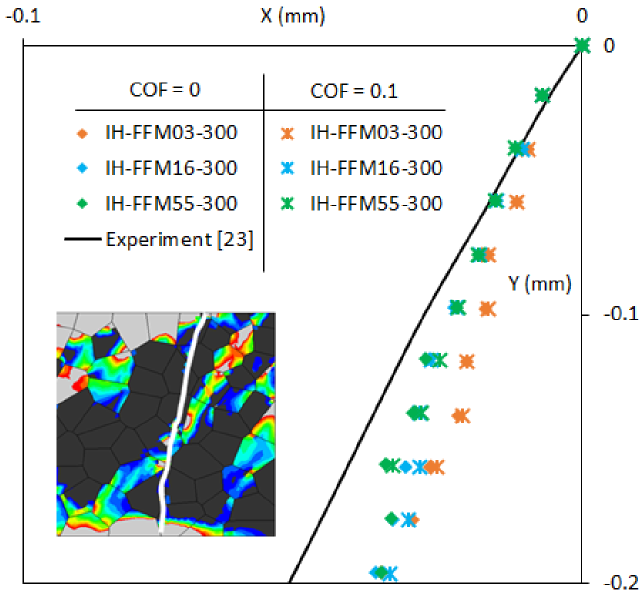

Figure 16. *The position of the crack tip in the conducted simulations with frictionless and penalty friction tangential contact, at the bulk stress level of 300 MPa, compared with the experimental crack path taken from* [51].